Electrochemically Induced Phase Transformation in Nanoscale Olivines $Li_{1-x}MPO_4$ (M = Fe, Mn)

Nonglak Meethong, Yu-Hua Kao, Ming Tang, Hsiao-Ying Huang, W. Craig Carter, and Yet-Ming Chiang*

Massachusetts Institute of Technology, 77 Massachusetts Avenue, Cambridge, Massachusetts

Received June 24, 2008. Revised Manuscript Received July 31, 2008

The phase stability and phase transformation kinetics of $Li_{1-x}MPO_4$ olivines are critical to their performance as lithium storage electrodes. In this work, nanoscale (<100 nm primary particle size) $Li_{1-x}FePO_4$ and $Li_{1-x}MnPO_4$ are chosen as model systems for comparison with a coarser-grained $LiFePO_4$ that exhibits a conventional two-phase reaction. The nanoscale materials first exhibit time and state-of-charge dependences of the electrochemical potential and structural parameters which show that stable two-phase coexistence is not reached. The evolution of structural parameters supports the existence of a coherency stress influenced crystal−crystal transformation. However, an additional response, the preferential formation of amorphous phase at nanosize scale, is identified. In $Li_{1-x}FePO_4$, at 34 nm average particle size, at least one amorphous phase of varying Li content coexists with the crystalline phases. In $Li_{1-x}MnPO_4$ of 78 nm particle size, the electrochemically formed delithiated phase is highly disordered. These phenomena are interpreted from the effect of surface and bulk energetics on phase stability of a nanoscale material.

Introduction

Although the applications for lithium transition metal olivine cathodes were initially uncertain due to their inferior energy density compared to, for instance, $LiCoO_2$, the recent commercialization of compositionally modified nanoscale olivines in applications such as cordless power tools[1] and hybrid electric vehicles (HEV)[2,3] suggests an important future role in high-power, safe, long-lived rechargeable batteries. In these applications, the phase behavior and phase transformation kinetics are critical, given that the equilibrium phase diagram shows limited solubility between the lithiated and delithiated phases[4−6] and requires a first-order phase transformation during electrochemical cycling. We previously documented several key differences in phase transformation behavior between conventional particle sized and nanoscale (<100 nm) olivine positive electrodes. With the use of electrochemical titration and structural (Vegard's law) measurements, it was shown that nanoscale (<50 nm) $Li_{1-x}FePO_4$ has a size-dependent, reduced miscibility gap compared to coarser-grained materials.[7] In doped nanoscale phosphates the miscibility gap is narrower still.[8,9] A size-dependent phase diagram has also been reported for Li−TiO_2 by Wagemaker et al.[10] In the olivines, it was furthermore shown that when the lattice mismatch between the coexisting lithium-rich and lithium-poor phases is sufficiently reduced, the phase transformation kinetics as measured by potentiostatic intermittent titration test (PITT) are qualitatively different than for samples of even slightly coarser size (113 nm) in which the coexisting phases have a larger misfit.[8] At small overpotentials, the latter show nucleation-limited behavior with phase transformation rates that increase slowly over many hours and cannot be modeled by any simple diffusion law,[11] while the doped nanomaterials show facile transformation with a rapid, monotonic decay in transformation rate. In combination with X-ray diffraction evidence for higher retained strain in the nanomaterials, it was proposed that relief of the misfit strain facilitates high rate capability.[8] It was suggested that reducing the elastic misfit was a fruitful approach to obtaining high ion-exchange rates in phase-transforming systems in general.

There may furthermore be differences in the way a single particle accommodates the phase transformation compared to a multiparticle assembly that is able to redistribute lithium between particles in order to reduce excess energy. Clearly a single particle that is partially transformed must accommodate both phases within the same crystallite, assuming

* Corresponding author. Phone: (617) 253 6471. Fax: (617) 253 6201. E-mail: ychiang@mit.edu.

(1) Macilwain, C. *Nature* **2006**, *444*, 17.
(2) Chu, A. Development of HEV Batteries with Lithium Iron Phosphate Cathodes. Presented at the Advanced Automotive Battery Conference, Baltimore, MD, June, 2006.
(3) http://www.A123Systems.com.
(4) Delacourt, C.; Laffont, L.; Bouchet, R.; Wurm, C.; Leriche, J. B.; Morcrette, M.; Tarascon, J. M.; Masquelier, C. *J. Electrochem. Soc.* **2005**, *152*, A913.
(5) Yamada, A.; Takei, Y.; Koizumi, H.; Sonoyama, N.; Kanno, R.; Ito, K.; Yonemura, M.; Kamiyama, T. *Nat. Mater.* **2006**, *5*, 357.
(6) Dodd, J. L.; Yazami, R.; Fultz, B. *Electrochem. Solid-State Lett.* **2006**, *9*, A151.
(7) Meethong, N.; Huang, H. S.; Carter, W. C.; Chiang, Y. M. *Electrochem. Solid-State Lett.* **2007**, *10* (5), A134.
(8) Meethong, N.; Huang, H. S.; Speakman, S. A.; Carter, W. C.; Chiang, Y. M. *Adv. Funct. Mater.* **2007**, *17* (7), 1115.
(9) Kao, Y.-H.; Meethong, N.; Tang, M.; Huang, H.-Y.; Carter, W. C.; Chiang, Y.-M. Presented at the International Meeting on Lithium Batteries−14, Tianjin, China, June 22−27, 2008; Abstract 14.
(10) Wagemaker, M.; Borghols, W. J. H.; Mulder, F. M. *J. Am. Chem. Soc.* **2007**, *129*, 4323.
(11) Levi, M. D.; Aurbach, D. *J. Solid State Electrochem.* **2007**, *11*, 1031.

10.1021/cm801722f CCC: $40.75
Published on Web 09/23/2008

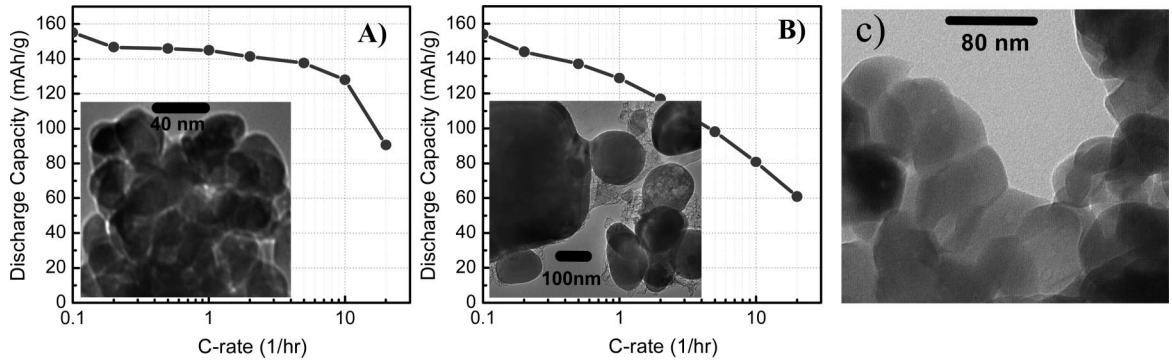

Figure 1. Three powders used in this study: (A) sample A, $Li_{1-x}FePO_4$ having 34 nm average particle size as determined from the BET specific surface area, (B) sample C, $LiFePO_4$ having 113 nm average size, and (C) sample M, $Li_{1-x}MnPO_4$ having 78 nm average particle size. The specific capacity vs C-rate is shown for samples A and C.

no fracture. However, a partially transformed multiparticle system can relax to a more energetically favorable assembly consisting of a mixture of single-phase particles of the two phases, since the retention of partially transformed particles possessing either coherency stresses or incoherent interfaces is metastable. Whether this state is achieved in practice depends on kinetics: the rate of lithium redistribution relative to the time scale on which the material is being electrochemically cycled. This led us to expect a possible evolution of the phase distribution over time in electrodes that are at a fixed overall composition (i.e., state of charge).

The increased surface area to volume ratio alone of nanoparticles may also lead to a contribution of surface defects or solute segregation to the observed phase behavior. To cite some previous examples, interfacial solute segregation has been observed to increase the "macroscopic" solubility limit of CaO in nanocrystalline TiO_2,[12] and increased nonstoichiometry has been observed in nanoscale CeO_{2-x} due to the lower oxygen vacancy formation enthalpy at interfaces.[13] The well-known formation of space-charges at surfaces and grain boundaries in ionic compounds also arises from the segregation of native defects or solutes.[14−16] Although the high bulk defect concentration of lithium intercalation compounds implies a very compact space-charge layer, changes in composition at the surface or the "core" of the grain boundary nonetheless will contribute to deviations in overall composition or nonstoichiometry if there is preferential segregation of solutes or defects.

These and other effects occurring in nanoscale intercalation compounds may be measurable through a combination of structural and electrochemical methods. We expected internal stress to be a function of the state of charge and time, possibly resulting in measurable changes in the lithium chemical potential. To explore this we measured the time and state-of-charge dependence of the open-circuit voltage (OCV, vs Li/Li^+) and the corresponding crystal lattice parameters in electrochemically cycled olivines. Nanoscale (defined as <100 nm primary particle size) $Li_{1-x}FePO_4$ is compared with a coarser-grained $LiFePO_4$ that serves as an example of the conventional two-phase reaction. The electrochemically induced transformation in $Li_{1-x}MnPO_4$ is examined as well. We find support for the coherency stress effect where each crystalline phase affects the structure and composition of the other. However, we also identify an additional response, which is the formation of a coexisting amorphous state upon cycling materials of nanosize scale. This tendency to disorder appears to be greater for $Li_{1-x}MnPO_4$ than for $Li_{1-x}FePO_4$. These phenomena are interpreted from the elastic misfit between coexisting phases and the effect of surface energetics on nanoscale phase stability.

Experimental Section

Model nanoscale materials of undoped $LiMPO_4$ compositions were selected for comparison. For examination of the lithium iron phosphate system we compared in detail two triphylite samples from a previous study representing the limiting cases of a "conventional" material and a nanoscale sample showing significant contraction of the miscibility gap.[7] Transmission electron microscopy (TEM) images and specific capacity versus C-rate tests of the samples studied are shown in Figure 1.

The nanoscale sample (sample A) has a specific surface area measured by the BET method (Brunauer, Emmett, and Teller) of 48.8 m^2/g, corresponding to an equivalent spherical particle diameter of 34 nm, and was synthesized as described in ref 17. In brief, Li_2CO_3, $FeC_2O_4 \cdot H_2O$ (or $MnCO_3$), and $NH_2H_2PO_4$, each assayed by the manufacturer or by us in order to determine the true metals content, were weighed in an Ar-filled glovebox (<3 ppm oxygen and water), then mixed by ball-milling in acetone for 24 h using zirconia milling media. The powder was dried and calcined at 350 °C for 10 h in flowing argon, then at 600−700 °C in flowing argon for 5 h. The crystallite size in sample A as derived from X-ray line broadening (Scherrer formula) was 32 nm, in good agreement with the measured specific surface area as well as the TEM images. The TEM results also show that the powder particles are equiaxed in shape, exhibiting no apparent faceting on any particular crystal plane. Sample A showed the smallest miscibility gap (largest mutual solid solubility) between the triphylite and heterosite phases in the previous study of undoped $Li_{1-x}FePO_4$, based on both X-ray measurements of lattice constants (Vegard's law) as well as electrochemical titration tests.[7] Sample C is a commercially purchased "carbon-added" $LiFePO_4$ (Aldrich Chemical) having 14.8

(12) Terwilliger, C. D.; Chiang, Y. M. *Acta Metall. Mater.* **1995**, *43* (1), 319.
(13) Chiang, Y. M.; Lavik, E. B.; Kosacki, I.; Tuller, H. L.; Ying, J. Y. *Appl. Phys. Lett.* **1996**, *69* (2), 185; *J. Electroceram.* **1997**, *1*, 7.
(14) Kliewer, K. L.; Koehler, J. S. *Phys. Rev. A* **1965**, *140*, 1226.
(15) Yan, M. F.; Cannon, R. M.; Bowen, H. K. *J. Appl. Phys.* **1983**, *54* (2), 764.
(16) (a) Ikeda, J. A. S.; Chiang, Y. M. *J. Am. Ceram. Soc.* **1993**, *76*, 2437. (b) Ikeda, J. A. S.; Chiang, Y. M.; Garratt-Reed, A. J.; Vander Sande, J. B. *J. Am. Ceram. Soc.* **1993**, *76*, 2447.

m^2/g specific surface area and 113 nm equivalent spherical particle diameter. TEM showed that this material had a broader particle size distribution than sample A as well as a clearly observable carbon phase. The specific discharge capacity versus C-rate performance of samples A and C are shown in Figure 1. A lithium manganese phosphate (lithiophilite) sample, sample M, was also examined in this study; this material was also made by the method of ref 17 and had a specific surface area of 22.2 m^2/g corresponding to an equivalent spherical diameter of 78 nm, consistent with the TEM imaging of this sample in Figure 1C.

Electrochemical tests were performed using electrodes formulated with 79 wt % positive active material, 10 wt % conductive carbon black (Super P, MMM Carbon, Brussels, Belgium), and 11 wt % Kynar 2801 binder, using acetone as the solvent. The formulation was coated onto aluminum foil current collectors at a loading of ~5 mg/cm^2 of active material and assembled in Swagelok-type cells using Li metal foil as the counter electrode, a microporous polymer (Celgard 2400, Hoechst Celanese Corporation, Charlotte, NC), and liquid electrolyte mixtures containing 1:1 by mole ethylene carbonate/dimethyl carbonate (EC/DMC) or ethylene carbonate/diethyl carbonate (EC/DEC), and 1 M $LiPF_6$ as the conductive salt. Arbin or Maccor instrumentation was used for the galvanostatic and potentiostatic tests.

For X-ray diffraction structural analysis of the electrochemically transformed materials, freshly assembled Swagelok cells were first galvanostatically cycled through two complete cycles. This was done at a *C*/10 rate at room temperature for samples A and C, from which the specific capacity of the material was established. Then, each cell was charged at the same rate to a percentage of the *C*/10 capacity corresponding to a desired state of charge (SOC). Thus, the SOC is here defined with respect to the practical capacity measured at the experimental voltage limits, rather than the theoretical capacity. Sample M was galvanostatically cycled at *C*/50 rate at 50 °C (due to its slower kinetics at room temperature), following which it was charged at the same rate to a desired SOC. A freshly assembled cell was used for each measurement of OCV or structure in order to avoid accumulating any history-dependent effects. Over the course of this study over 100 cells were constructed and tested. For the lithium iron phosphate samples the cycling voltage limits were 2.0−4.2 V, whereas for the lithium manganese phosphate it was 2.0−4.5 V.

To measure the equilibrium OCV as a function of the SOC, cells were galvanostatically charged or discharged to the desired SOC, and then the OCV was allowed to relax for 200 h, after which the rate of voltage decay, dV/dt, was less than 10^{-7} V/h. These measurements were carried out with the cells being held in a temperature-controlled oven at 22 ± 0.2 °C. The voltage was measured to 0.1 mV resolution. The average OCV measured at 1 h intervals over the last 20 h was used as the equilibrium or "fully relaxed" electrical potential.

For measurement of structure by X-ray diffraction as a function of the SOC, cells were galvanostatically charged or discharged to a desired SOC, then immediately disassembled in an argon-filled glovebox. The positive electrodes of sample C were mounted on an aluminum sample holder for X-ray diffraction. X-ray patterns were obtained using a Rigaku RTP500RC instrument with a rotating anode and Cu Kα radiation, at a slow can rate of 0.18°/min over a 2θ range from 15° to 135°. For nanocrystalline samples A and M, the delithiated phases were found to be very sensitive to air exposure, exhibiting an exposure-related loss of crystallinity that may be due to reaction with air-borne water. In order to exclude such effects, X-ray diffraction (XRD) spectra were obtained using sample holder designed by the manufacturer for air-sensitive samples, which we sealed using 2 layers of 7.5 μm thick Kapton tape. These samples were characterized using Cu Kα X-rays and the PANanalytical X'Pert PRO XRD system using a slow scan rate of 0.15°/min over a 2θ range from 15° to 135°. Control experiments were conducted which showed that the cycled samples did not change over the time scale of the measurements. The structural parameters of all X-ray data were refined by Rietveld analysis using PANalytical X'Pert HighScore Plus software, and the backgrounds were manually fitted. Note that the backgrounds for the electrodes will include contributions from the binder, electrolyte, and possibly side reaction products. As a result, the appearance of amorphous phases upon cycling of the active materials can be difficult to detect. We instead used crystalline phase fractions quantified by careful Rietveld refinement of high-quality X-ray spectra obtained in slow scan experiments carried out at various SOC. For the spectra obtained from sample C, the best estimate residual parameter (R_{exp}) and weighted residual profile error parameter (R_{wp}) values were less than 2.0% and 7.0%, respectively, indicating excellent data quality and reliable refinements. For the spectra obtained from sample A, the background profiles also included contributions from the Kapton tape and therefore the signal-to-noise was slightly worse. Nonetheless, R_{exp} and R_{wp} for sample A were still less than 3.0% and 12.0%, respectively, again indicating high data quality and reliable refinements. Crystalline size and microstrain were determined using the Williamson−Hall analysis, and NIST silicon 640c was used as an external standard.

Results and Discussion

Time and State-of-Charge Dependence of OCV. In the conventional view of intercalation compounds undergoing a two-phase reaction, the lithium chemical potential is pinned at a constant value (at constant temperature and pressure) as required by the Gibbs phase rule, and the positive electrode potential relative to Li/Li^+ should theoretically be constant across the two-phase coexistence field. This was found not to be true in the present materials when the OCV is examined at a submillivolt scale of resolution. For sample A, panels A and B in Figure 2 show the time dependence of OCV after charging and discharging, respectively, to various SOC (or state of discharge, SOD) between 20% and 80%. There is a clear relaxation of the OCV that takes place over tens of hours. This is remarkable given that sample A can be effectively cycled at rates >10*C* (Figure 1), which corresponds to roughly a 1×10^4 shorter time constant and suggests that the phase assemblage produced by electrochemical cycling is metastable. This phase assemblage nonetheless clearly has high lithium exchange rate. It is also seen that the OCV is not in fact constant with composition but increases with SOC in sample A. For sample C, the OCV relaxation during charging to various SOC is shown in Figure 2C. Here also, a relaxation of the OCV over 20−40 h as well as an SOC dependence is observed. However, the relaxation occurs faster for sample C, and the variation of OCV with SOD is weaker and has opposite sign to that in sample A.

To compare the composition range over which the OCV varies with the phase diagram of the respective materials, we plot in Figure 3A the temperature-dependent miscibility data for samples A and C from ref 7, as well as the equilibrium phase diagram of Dodd et al.[6] for bulk $Li_{1-x}FePO_4$. The dramatic shrinking of the miscibility gap at nanoscale particle size is clearly seen here.

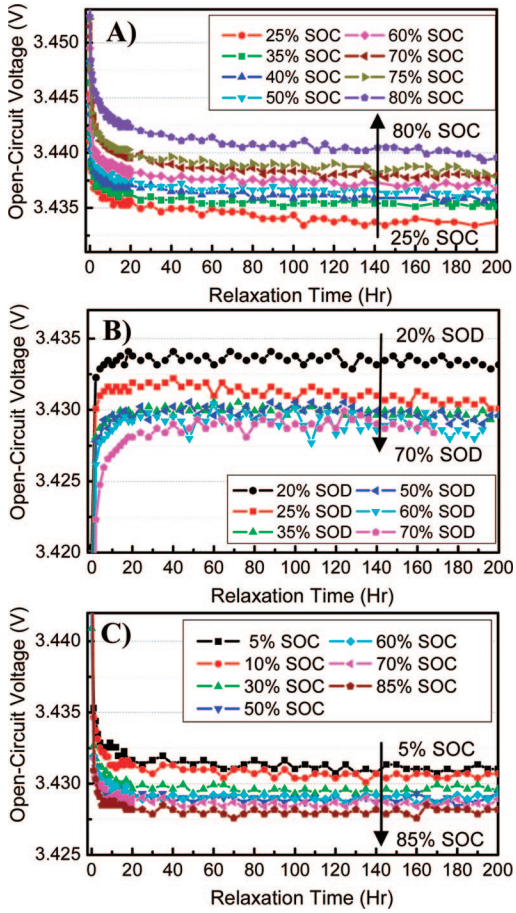

Figure 2. Time dependence of OCV of (A) sample A after charging to various states of charge (SOC), (B) sample A after discharging to various states of discharge (SOD), and (C) sample C after charging to various SOC. A relaxation of the OCV that takes place over as long as 100 h is seen in sample A, and over 20−40 h for sample C. The relaxed value of OCV is seen to be a function of SOC and SOD.

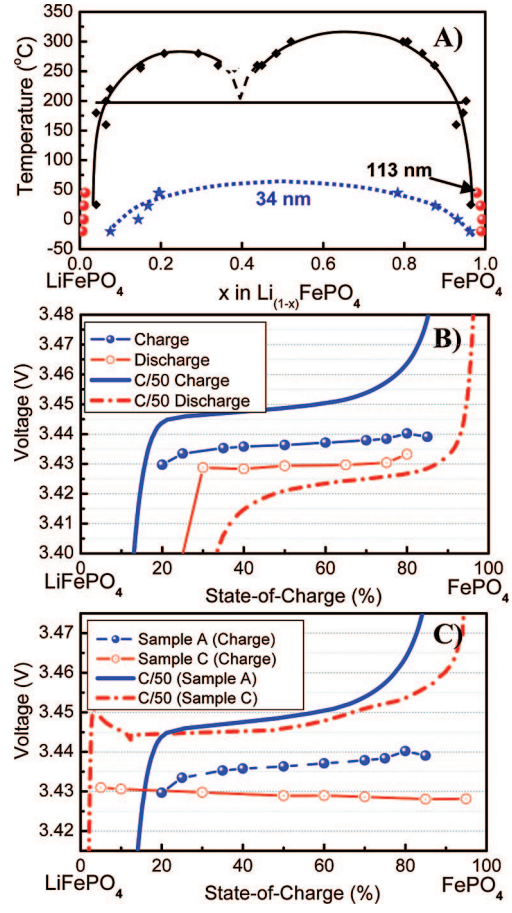

Figure 3. (A) Temperature-dependent miscibility data for samples A and C from ref 7 plotted against the equilibrium phase diagram of Dodd et al. (ref 6). (B) Room-temperature terminal OCV and galvanostatic voltage curve at *C*/50 rate measured on both charging and discharging of sample A. (C) Terminal OCV and *C*/50 galvanostatic charge curves measured at room temperature as a function of state of charge (SOC) for samples A and C.

The terminal (fully relaxed) OCV for sample A at room temperature is shown as a function of SOC in Figure 3B. Results for both charge and discharge are shown, and galvanostatic curves for the same material measured upon charge and discharge at a *C*/50 rate are also plotted for comparison. The SOC range of 30−75% lies within the room-temperature miscibility gap. The OCV measured upon both charge and discharge shows a slight increase with increasing SOC within the miscibility gap. There is also a hysteresis in the OCV between charge and discharge of about 7 mV. The variations in OCV seen here is much greater than can be accounted for by temperature variation during the experiment. For comparison, in ref 7 we measured the OCV of sample A at 50% SOC and temperatures ranging from −20 to +45 °C and found it to vary by 3 mV over this temperature range. The variation in OCV with SOC of sample A, shown in Figure 3A, is ∼10 mV despite temperature being constant to ±0.2 °C. Thus, the OCV variation cannot be attributed to temperature variation. Figure 3C shows the relaxed OCV and the *C*/50 galvanostatic curve for sample C compared to those for sample A. The wider SOC range over which the OCV is shown corresponds to the wider miscibility gap (Figure 3A). However, sample C also shows a measurable variation of OCV with SOC. Interestingly, it has the opposite slope, with the OCV decreases with increasing SOC. Furthermore, within its miscibility gap, sample C has a lower OCV by between 5 and 10 mV than sample A, which at room temperature corresponds to a difference in lithium chemical potential of 500−1000 J/mol. Clearly, the coexisting phase assemblages and/or compositions are not identical in samples A and C during electrochemical cycling.

State-of-Charge Dependence of "Triphylite" and "Heterosite" Phase Fractions. We next compare the evolution of the lithium-rich ("triphylite") and lithium-poor ("heterosite") phase fractions as a function of SOC in samples A and C, as determined by Rietveld refinement of the XRD spectra. The compositions of both phases can be nonideal; consistent with previous notation[7,8] we will use $Li_{1-x}FePO_4$ to denote the lithium-rich endmember having a lithium deficiency x with respect to its ideal composition (e.g., triphylite or lithiophilite) and Li_yFePO_4 to denote the lithium-poor endmember having a lithium excess y with respect to its ideal composition (e.g., heterosite or purpurite). The evolution of phase fractions in sample C followed nearly ideal two-phase behavior. Figure 4a shows a sequence of XRD spectra taken as a function of SOC from starting material through 95% SOC. The systematic variation in intensity of the heterosite (200), (201), and (301) peaks (labeled "H") relative to the same peaks for triphylite (labeled

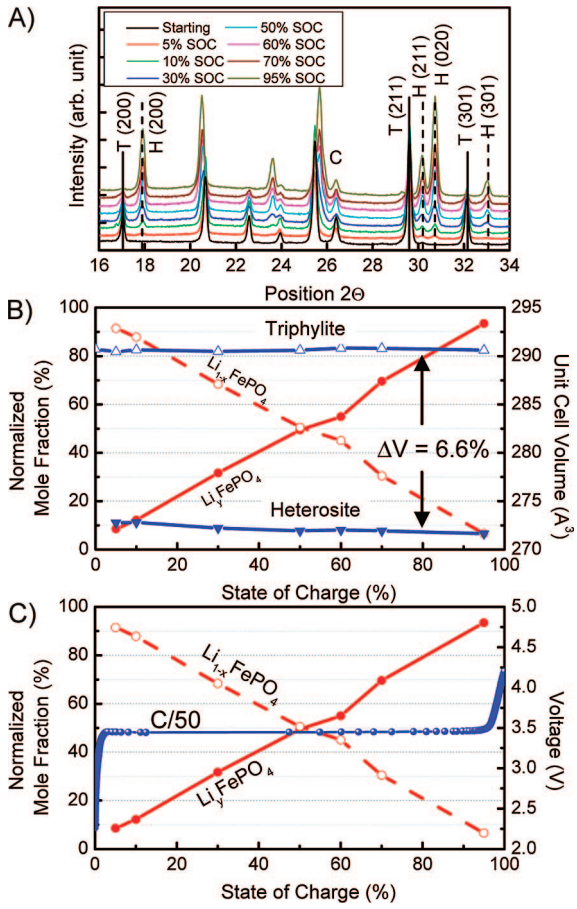

Figure 4. Results for sample C showing nearly ideal two-phase reaction. (A) XRD spectra taken as a function of state of charge (SOC) from starting material to 95% SOC with "H" representing heterosite, "T" representing triphylite, and "C" denoting the graphite (002) reflection from carbon additive in the electrode formulation. Only a portion of the full spectra obtained from 15° to 135° 2θ are shown. (B) Unit cell volumes and the normalized crystalline phase fraction of triphylite (unfilled symbols) and heterosite (filled symbols). (C) Galvanostatic voltage curve at *C*/50 measured at room temperature.

"T") with SOC is clearly seen. "C" refers to the (002) peak of graphite, resulting from the carbon additive used in the electrode formulation. Even at 5% and 95% SOC, the minority phases heterosite and triphylite, respectively, were readily detected. Figure 4b shows the evolution of the triphylite and heterosite phase fractions between 5% and 95% SOC, obtained by Rietveld refinement of X-ray spectra taken after 200 h of relaxation time. They vary linearly with SOC, as expected from the ideal two-phase model. The unit cell volumes determined from Rietveld refinement of the triphylite and heterosite structure as a function of SOC are also shown in Figure 4b. Note that the triphylite unit cell volume remains essentially constant across the entire SOC range; there is no evidence for induced nonstoichiometry x upon formation of the heterosite phase. However, the heterosite unit cell volume is measurably higher when the phase is first nucleated, then decreases with increasing SOC. We attribute this behavior to size and strain effects. Since the initially nucleated Li_yFePO_4 will have finer length scale and/or different morphology than the triphylite phase, it may be expected to have higher lithium nonstoichiometry y if, for example, coherency stresses are initially present between the parent triphylite and nucleated heterosite phase. As the heterosite fraction grows, the evolution of unit cell volumes shows that both phases become "fully relaxed" and approach limiting values consistent with previous literature data for these two compounds as bulk phases. The microstrain obtained from Rietveld refinement was consistent with this interpretation, with the triphylite phase having ~0.05% strain across the SOC range, whereas the heterosite phase had an initially higher microstrain of 0.15% when first measured at 5% SOC, declining to 0.09% by 50% SOC, and remaining at that value to 95% SOC. The difference in unit cell volume approaches 6.6%, which is typical of coarse-grained $Li_{1-x}FePO_4$.[7,8]

In Figure 4c, we compare the normalized mole fractions of triphylite and heterosite with the *C*/50 galvanostatic voltage curve for sample C. The deviations in voltage at the very beginning and end of charge corresponding to the formation of heterosite and disappearance of triphylite are seen. With the exception of the deviation in unit cell volume when the heterosite phase first forms, sample C behaves in a manner completely consistent with the conventional two-phase reaction viewpoint. The slight decrease in OCV as the heterosite unit cell volume relaxes to its bulk value indicates that the Li chemical potential is actually slightly higher (OCV lower) when both phases are fully relaxed.

Figure 5 shows that the phase-evolution behavior is markedly different for the nanocrystalline material, sample A. X-ray diffraction spectra for this sample as a function of SOC from starting material through 100% SOC are shown in Figure 5a. Here, 100% SOC corresponds to the extraction of lithium from a fully lithiated (discharged) material to a specific capacity of 155 mA h g^{-1} The higher background is due to the Kapton tape used to hermetically seal the sample holder.

The normalized phase fractions of $Li_{1-x}FePO_4$ and Li_yFePO_4, these being the only detectable crystalline phases aside from the carbon additive, are shown in Figure 5b as a function of SOC, along with their unit cell volumes. The nonstoichiometry parameters x, y calculated from Vegard's law are also given next to each unit cell volume datum. The triphylite $Li_{1-x}FePO_4$ unit cell volume decreases monotonically with increasing SOC even at compositions within the miscibility gap where two crystalline phases are present. The decreasing unit cell volume corresponds to increasing lithium deficiency x in the $Li_{1-x}FePO_4$ phase. Note that with increasing SOC, there is a small but sudden decrease in the unit cell volume of $Li_{1-x}FePO_4$ occurring concurrently with the first appearance of the heterosite Li_yFePO_4 crystalline phase at ~30% SOC. The initial Li_yFePO_4 formed at 25−30% SOC also has slightly larger unit cell volume, corresponding to larger lithium concentration ($y \sim 0.139-0.146$) than it does at higher SOC values ($y \sim 0.130-0.140$). At 100% SOC, the Li_yFePO_4 unit cell volume reaches its minimum value, as expected. The difference in unit cell volume at intermediate SOCs when both phases coexist is about 5.2%, significantly lower than for the coarse-grained sample C. The microstrain obtained from Rietveld refinement was significantly higher across the entire SOC range than for sample C, consistent with the presence of coherency stresses.[8] The microstrain in the $Li_{1-x}FePO_4$ phase was in

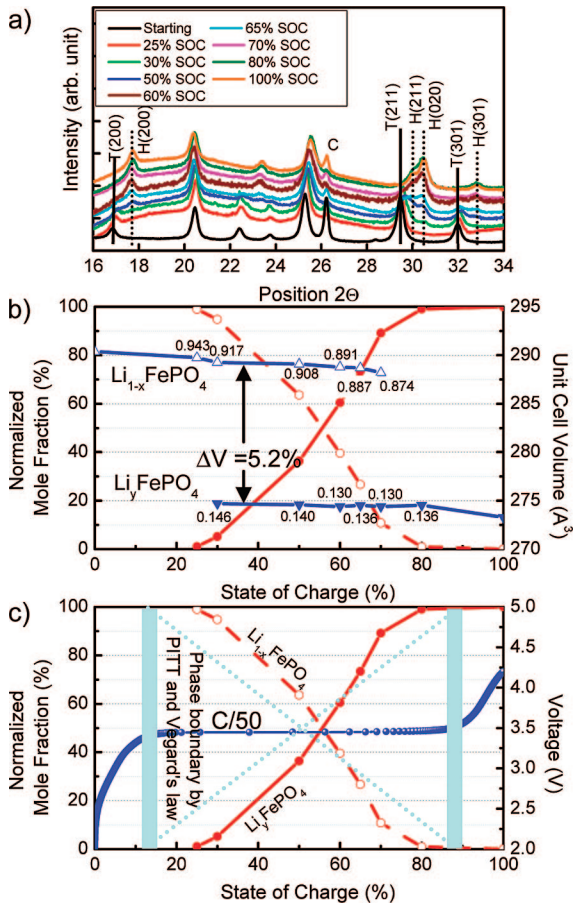

Figure 5. Results showing phase evolution in nanocrystalline sample A. (a) XRD spectra taken as a function of state of charge (SOC), from starting material to 100% SOC. Only a portion of the full spectra obtained from 15° to 135° 2θ are shown. (b) Unit cell volumes and the crystalline phase fraction of Li_yFePO_4 (filled symbols) and $Li_{1-x}FePO_4$ (unfilled symbols). The nonstoichiometry parameters x and y calculated from Vegard's law are given next to each unit cell volume datum. (c) Galvanostatic voltage curve measured at *C*/50 rate at room temperature. The phase boundaries measured in ref 7 by electrochemical (PITT) and XRD (Vegard's law) techniques are shown as shaded vertical lines.

the range of 0.2−0.3%, whereas that in the Li_yFePO_4 phase varied from 0.2% to 0.5%.

At the beginning and end of charge when only a single phase exists, we expect the unit cell volume to vary continuously due to the existence of a single-phase field. Judging from the SOC values at which the minor phase is first detected by XRD in Figure 5, the solid solution fields extend to $x \sim 0.25$ and $y \sim 0.2$, respectively, which are larger values than are observed for the same sample after charging to 50% SOC and allowing a long period of rest.[7] Within the miscibility gap, however, the present data indicate a significant new result: even in two-phase coexistence, the compositions evolve continuously. This is completely consistent with the results above (Figure 3) showing that the OCV varies with SOC continuously within the two-phase field. The initial decrease in $Li_{1-x}FePO_4$ unit cell volume when Li_yFePO_4 nucleates, the continuous variation over the SOC range where they coexist, and the smaller difference in unit cell volume when both phases coexist as compared to sample C are all consistent with the coherency stress model[7,8] in which the mechanical constraint imposed by each phase upon on the other causes their respective lattice constants (and lithium concentrations) to approach one another due to Vegard's stresses. Thus, in sample A, the compositions of the crystalline fractions behave as we have described previously.[7]

However, further anomalous behavior becomes evident when the phase fractions are quantified. In Figure 5c, the crystalline phase fractions and the *C*/50 galvanostatic charge curve for sample A are shown as a function of SOC. The boundaries of the miscibility gap at this temperature are drawn as broad vertical lines, encompassing the range of numerical values determined from PITT measurements and Vegard's law.[7] The phase fractions shown are the Rietveld-refined results for the two crystalline phases. It is seen that the variation of phase fraction with SOC is nonlinear, namely, in violation of the lever rule for coexistence of two phases within a fixed immiscibility field. Specifically, there is a deficiency of Li_yFePO_4 relative to that expected from the lever rule below 60−65% SOC and an excess above. The converse is true for the crystalline Li_yFePO_4 phase, the behavior of which is furthermore anomalous in that it is not detected until the sample reaches 25% SOC, a composition that is well within the crystalline miscibility gap determined in the previous study.[7] (In contrast, this phase was clearly detectable in sample C at 5% SOC, Figure 4.) The triphylite $Li_{1-x}FePO_4$ phase also disappears by 80% SOC, before the Li-rich phase boundary is reached.

Additional Amorphous or Disordered Phases. With the use of the graphite (002) peak from the carbon additive as a qualitative internal standard (Figures 4a and 5a), we had noted that the integrated intensity of the crystalline phase peaks in sample A appeared to be much lower than that in sample C. Given the nearly identical specific capacities of the two samples at *C*/5 rate (Figure 1), this alone suggested a substantial noncrystalline fraction in sample A. TEM analysis of the samples indeed showed the presence of amorphous particles, but we could not rule out the possibility that these formed upon exposure to air. However, quantification of the amount of amorphous or disordered phase was possible because we had experimental measurements of three independent quantities: (1) the crystalline phase compositions, via the unit cell volumes, (2) the crystalline phase fractions from Rietveld refinement of the diffraction data, and (3) the overall Li concentration from electrochemical cycling. One may then apply mass balance relationships to determine the amount or concentration of the noncrystalline phases. The simplest such relationship assumes a single amorphous phase α-Li_zFePO_4 coexisting with the two observed crystalline phases. At a given SOC where the overall composition is $Li_\beta FePO_4$, mass balance requires that

$$a\mathrm{Li}_{1-x}\mathrm{FePO}_4 + b\mathrm{Li}_y\mathrm{FePO}_4 + c\alpha\text{-}\mathrm{Li}_z\mathrm{FePO}_4 = \mathrm{Li}_\beta\mathrm{FePO}_4 \quad (1)$$

where a, b, and c are the molar fractions of each respective phase ($a + b + c = 1$) and lithium mass balance is given by $(1 - x)a + yb + zc = \beta$. We currently do not know z and c independently but can place bounds on the product zc. For example, taking $(1 - x) = 0.91$ and $y = 0.14$, representing the results in Figure 5 at 50% SOC (with the ratio of $Li_{0.91}FePO_4$ phase to $Li_{0.14}FePO_4$ phase of ~2:1) if the amorphous phase is assumed to be completely delithiated (z

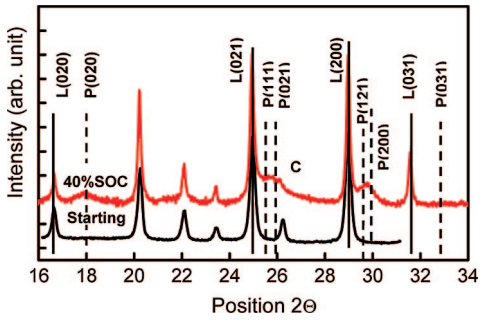

Figure 6. XRD spectra of sample M in its starting state and after charging to composition $Li_{0.60}MnPO_4$. The sample exhibits broadened peaks for the delithiated Li_yMnPO_4 (labeled "P") phase indicating that the newly formed phase is highly disordered.

= 0), then at 50% SOC there is 51 mol % of $Li_{0.91}FePO_4$, 26 mol % of $Li_{0.14}FePO_4$, and 23 mol % of the amorphous phase α-$FePO_4$. This is a substantial fraction of amorphous phase. If the amorphous phase is assumed to be partially lithiated, then its molar percentage will be even higher than this limiting value. For example, if the amorphous phase is assumed to have composition $Li_{0.2}FePO_4$, then at 50% SOC we have 44 mol % of $Li_{0.91}FePO_4$, 22 mol % of $Li_{0.14}FePO_4$, and 34% of the amorphous phase α-$Li_{0.2}FePO_4$.

The curves for the crystalline phase fractions versus SOC in Figure 5 have a sigmoidal shape, crossing the straight lines that define the two-phase lever rule at between 60% and 65% SOC. This means that only in this narrow range of composition is it possible to explain the overall composition β from a mixture of the two crystalline phases alone. (Coexistence of an amorphous phase is not ruled out, however.) Below this SOC, there is a deficiency of the delithiated phase Li_yFePO_4, and mass balance requires the presence of an additional noncrystalline delithiated phase. Above this SOC, there is a deficiency of the lithiated phase $Li_{1-x}FePO_4$, and the noncrystalline phase must be substantially lithiated to satisfy mass balance. It is unlikely that there is such a complex evolution where at low SOC there is first a delithiated amorphous phase, then no amorphous phase at 60−65% SOC, and finally a lithiated amorphous phase at higher SOC. Instead, we believe that an amorphous phase is present throughout, in which the lithium concentration z increases systematically with SOC. The amount of noncrystalline phase required to satisfy mass balance is in general well beyond that which can be provided by a surface atomic layer alone, given the surface to volume ratio of these powders. Thus, we do not believe the results can be explained by surface enrichment or depletion of lithium at sites having a different chemical potential than the bulk, although the amorphous phase may well form as a surface coating, as discussed later. Detailed knowledge of the amorphous phase composition will allow a more precise estimate of the phase fractions. It is also possible that more than one noncrystalline phase is present.

Phase Transformation upon Cycling of Nano-$Li_{1-x}MnPO_4$. Experiments were also conducted on LiMnPO$_4$, sample M, in which we expected an even greater tendency toward amorphization for reasons discussed later. Figure 6 shows X-ray patterns from the sample in its starting state and after charging to 40% SOC at *C*/50 rate and 50 °C. The sample was first given two complete cycles under these conditions. "L" and "P" in Figure 6 refer to lithiophilite and purpurite, the lithium-rich and lithium-poor endmembers of this system, respectively. "C" again refers to the (002) peak of graphite, resulting from the carbon additive used in the electrode formulation. It can be seen that the peaks for the delithiated Li_yMnPO_4 phase after charging are extremely broad, indicating that the newly formed phase is highly disordered if not amorphous.

General Discussion

The observed behavior of these crystalline olivines at nanoscale particle sizes bears similarities to several other surface and nanoscale phenomena in which a disordered noncrystalline phase, despite having higher volume free energy, is stabilized under the influence of surface energy, mechanical stress, or other short-range interactions. In surface premelting, which is best known for ice[18−20] but also occurs in certain elemental metals,[21] the surface of a crystal begins to melt below the bulk melting point (by ∼2 K for ice) due to the lower surface energy of the liquid compared to the crystal. The premelted layer is constrained in its thickness by the increase in volumetric energy upon thickening as well as by dispersion interactions across the nanometer-thick film. Similar effects cause melting point suppression in nanocrystalline metals.[22,23] The surface-energy-stabilized disordered phase may be a glass rather than a liquid. In binary oxides, nanometer-thick solid amorphous films of compositions that do not appear in the bulk phase diagram are stabilized on crystalline oxide surfaces for similar reasons.[24−26] These films also take on nanometer-scale thickness, as they are prevented from thickening further by their higher volume free energy compared to the crystal. Intergranular amorphous films of similar character have been widely reported; note that these are not "wetting" liquids in the conventional sense but disordered solid films that form to minimize interfacial energy.[27−29] Thus, a nanoparticle system which has a lower surface energy for its glass than the corresponding crystal should become amorphous with decreasing size (increasing surface to volume ratio), first at the surface of the particle and eventually stabilizing the entire particle in the glassy state. This phase conversion has been shown in nanocrystalline zirconia,[30] where high-temperature oxide melt solution calorimetric measurements confirm the existence of a phase stability crossover from the bulk-stable monoclinic phase to

(17) Chung, S.-Y.; Bloking, J. T.; Chiang, Y.-M. *Nat. Mater.* **2002**, *1*, 81.
(18) Dash, J. G. *Contemp. Phys.* **1989**, *30*, 89.
(19) Dash, J. G.; Fu, H.; Wettlaufer, J. S. *Rep. Prog. Phys.* **1995**, *58*, 115.
(20) Dash, J. G.; Rempel, A. M.; Wettlaufer, J. S. *Rev. Mod. Phys.* **2006**, *78*, 695.
(21) Frenken, J. W. M.; van der Veen, J. F. *Phys. Rev. Lett.* **1985**, *54*, 134.
(22) Buffat, Ph.; Borel, J. P. *Phys. Rev. A* **1976**, *13* (6), 2287.
(23) Schebarchov, D.; Hendy, S. C. *Phys. Rev. Lett.* **2006**, *96*, 256101–1.
(24) Luo, J.; Chiang, Y.-M. *Acta Mater.* **2000**, *48*, 4501.
(25) Luo, J.; Chiang, Y.-M.; Cannon, R. M. *Langmuir* **2005**, *21*, 7358.
(26) Luo, J. *Crit. Rev. Solid State Mater. Sci.* **2007**, *32*, 67.
(27) Cannon, R. M.; Esposito, L. *Z. Metallkd.* **1999**, *90*, 1002.
(28) Kleebe, H.-J.; Cinibulk, M. K.; Cannon, R. M.; Ruhle, M. *J. Am. Ceram. Soc.* **1993**, *76*, 1969.
(29) Clarke, D. R.; Shaw, T. M.; Philipse, A. P.; Horn, R. G. *J. Am. Ceram. Soc.* **1993**, *76*, 1201.
(30) Pitcher, M. W.; Ushakov, S. V.; Navrotsky, A.; Woodfield, B. F.; Li, G.; Boerio-Goates, J.; Tissue, B. M. *J. Am. Ceram. Soc.* **2005**, *88*, 160.

metastable tetragonal and then amorphous phases with increasing specific particle surface area.

The present metal phosphates do appear to readily form disordered solids. Like other "III−V" analogues to SiO_2, such as $AlPO_4$,[31,32] $FePO_4$ is stable at atmospheric pressure in the quartz structure[33] but is a good glass former. Iron phosphate glasses are readily made by quenching from the melt,[34] and amorphous anhydrous $FePO_4$ is readily formed by heating of $FePO_4 \cdot nH_2O$, retaining an amorphous structure until about 500 °C.[35−38] The latter can also be chemically lithiated without crystallization.[37] Thus, the volume free energy difference between the glassy and crystalline form of $FePO_4$ appears to be relatively small. $MnPO_4$ is less well studied but should behave similarly. As with SiO_2, a glass structure that is in general a continuous random network consisting of corner-linked oxygen tetrahedra[38] alternatively filled with Fe^{3+} (or Mn^{3+}) and P^{5+} seems likely. Upon lithiation, the present experimental data as well as ref 37 indicate retention of the glassy structure, which may correspond to Li^+ in interstitial positions like those occupied by alkali ions in common alkali-modified silicates,[39] charge compensation being provided by the Fe^{3+} in tetrahedral coordination. However, the disordered structures of melt-quenched, dehydrated, and electrochemically transformed disordered structures (the present case) may differ significantly in the details of their short-range order. In $AlPO_4$, what was thought to be a simple crystal-to-glass transition under high pressure was later shown to be, first, a transition to a disordered crystalline phase with short-range order, prior to true amorphization at higher pressures.[31] The electrochemically driven crystal-to-amorphous transition in the present materials may also have complex behavior.

Glassy $FePO_4$ and $MnPO_4$ should be structurally similar in local coordination to their quartz isomorphs in the same way that amorphous SiO_2 is similar to quartz. If so, they should have generally lower surface energy than their crystalline counterparts. Parks[40] compared the interfacial energies of quartz and amorphous silica based on their solubilities in aqueous solutions (Gibbs−Thomson effect) and found a difference of $\sim$0.3 J/m^2. For the free surfaces, an even larger difference is implied if the dehydroxylation energy is included. The surface energy of liquid SiO_2 extrapolated from high-temperature data to room temperature is $\sim$0.3 J/m^2,[40] whereas the fracture surface energy of quartz ranges from $\sim$0.4 (for $(10\bar{1}1)$ and $(\bar{1}011)$ orientations) to $\sim$1 J/m^2 ($(10\bar{1}0)$ and $(11\bar{2}0)$ orientations). Because of the isotropic shape of the present particles (Figure 1) the relevant comparison is between the amorphous glass surface and an orientational average of crystalline surface energies, which in the case of SiO_2 is a difference of at least 0.3 J/m^2.

The avoidance of coherency stresses[8] is another factor that will promote amorphization. Consider a crystalline particle that is undergoing delithiation and for which substantial crystalline misfit stresses must be accommodated if it is to transform according to the conventional two-phase reaction model. The particle may (1) form an incoherent interface between the $Li_{1-x}MPO_4$ and Li_yMPO_4 phases and accept a higher interfacial energy as the penalty for relieving lattice strain energy, (2) form a coherent interface of lower energy and accommodate the misfit as lattice strain and corresponding deviations in the coexisting phase compositions, or (3) simultaneously relieve the interfacial energy by forming a crystal−glass interface and the volume strains by forming the amorphous phase. Between the present work and previous publications,[7,8] we have evidence for each mode of behavior occurring depending on the specific material in question. $LiMnPO_4$ is clearly more prone to amorphization upon delithiation than $LiFePO_4$. Although a complete understanding of the differences between these two compounds requires additional data on the volumetric and surface energies involved, a contributing factor may be the much larger crystalline misfit in the $LiMnPO_4$−$MnPO_4$ system, 11% difference in unit cell volume for the stoichiometric compositions.[8] In elemental silicon, which also adopts a continuous-random-network glassy structure,[41] the structural misfit between parent phase and lithiated intermetallic compounds is even larger than in the present materials, and a previous study has shown that lithiation of crystalline Si results in solid-state amorphization as well.[42]

The several possible phase transformation pathways between lithiated and delithiated phases elucidated by the present work are illustrated in Figure 7. A coarse, single-crystalline particle that is effectively isolated from any neighbors undergoes conventional nucleation and growth, with the multiphase particle having excess interfacial and strain energy in the partially transformed state (Figure 7A). In general, the morphology will not be of a "core−shell" configuration due to the influences of anisotropy in elastic constants, diffusion, or surface energy.[8,43] In a multiparticle assembly (Figure 7B), the same partially transformed state may initially occur. This state, however, is metastable with respect to a two-phase mixture of single-phase particles in which coherency strain and interfacial energies are removed. Whether the end point in Figure 7B is reached depends on kinetics; for example, the two-phase particles observed by

(31) Gillet, Ph.; Badro, J.; Varrel, B.; McMillan, P. F. *Phys. Rev. B* **1995**, *51*, 262.
(32) Gutiérrez-Mora, F.; Goretta, K. C.; Singh, D.; Routbort, J. L.; Sambasivan, S.; Steiner, K. A.; Adabie, J.; Rangan, K. K. *J. Eur. Ceram. Soc.* **2006**, *26*, 1179.
(33) Aliouane, N.; Badechet, T.; Gagou, Y.; Nigrelli, E.; Saint-Gregoire, P. *Ferroelectrics* **2000**, *241*, 255.
(34) Friebele, E. J.; Wilson, L. K.; Dozier, A. K.; Kinser, D. L. *Phys. Status Solidi A* **1971**, *45*, 323.
(35) Hong, Y. S.; Ryu, K. Y.; Park, Y. J.; Kim, M. G.; Lee, J. M.; Chang, S. H. *J. Mater. Chem.* **2002**, *12*, 1870.
(36) Song, Y.; Yang, S.; Zavalij, P. Y.; Whittingham, M. S. *Mater. Res. Bull.* **2002**, *37*, 1249.
(37) Prosini, P. P.; Lisi, M.; Scaccia, S.; Carewska, M.; Cardellini, F.; Pasqualib, M. *J. Electrochem. Soc.* **2002**, *149* (3), A297.
(38) Okada, S.; Yamamoto, T.; Okazaki, Y.; Yamaki, J.; Tokunaga, M.; Nishida, T. *J. Power Sources* **2005**, *146*, 570.
(39) Chiang, Y.-M.; Birnie, D. P., III; Kingery, W. D. *Physical Ceramics*; John Wiley and Sons: New York, 1997.
(40) Parks, G. A. *Rev. Mineral.* **1990**, *23*, 133.
(41) Zallen, R. *Physics of Amorphous Solids*; J. Wiley and Sons: New York, 1983.
(42) Limthongkul, P.; Jang, Y. I.; Dudney, N.; Chiang, Y. M. *Acta Mater.* **2003**, *51*, 1103.
(43) Chen, G.; Song, X.; Richardson, T. *Electrochem. Solid-State Lett.* **2006**, *9*, A295.
(44) Delmas, C.; Maccario, M.; Croguennec, L.; Wattiaux, A.; Le Cras, F.; Weill, F. Presented at the 212th Electrochemical Society Meeting, Washington, DC, 2007; Abstract No. 270.

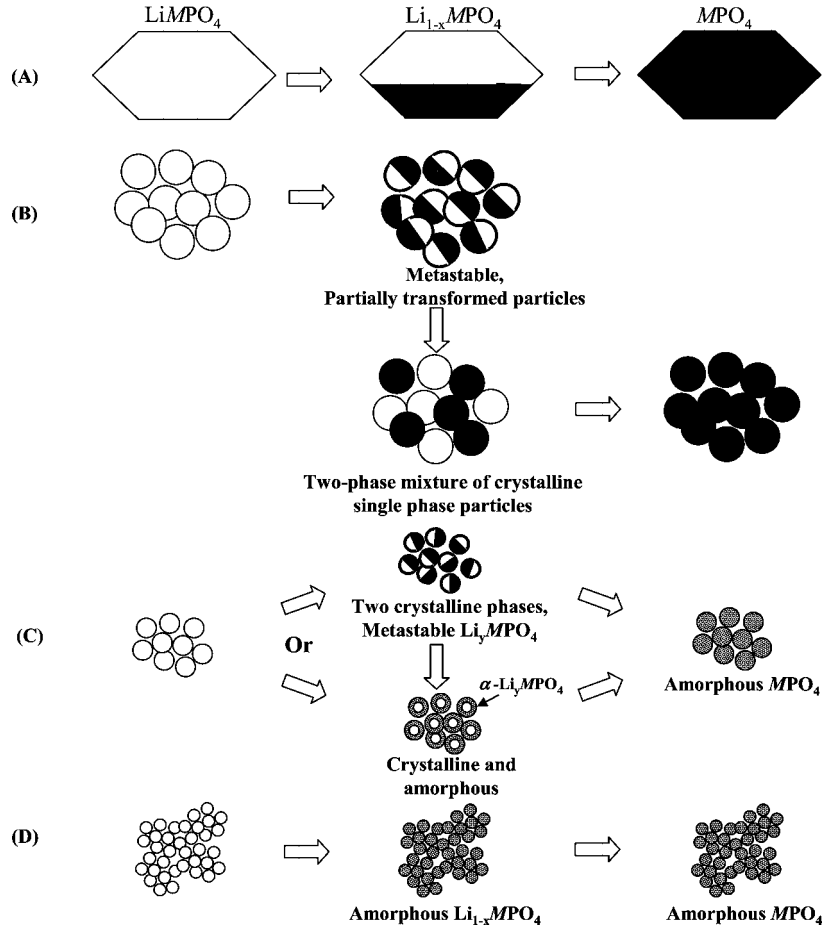

Figure 7. Phase transformation pathways between lithiated and delithiated phases in $LiMPO_4$ olivines.

Chen et al.[43] are clearly frozen in the partially transformed state. The metastability of a delithiated olivine with respect to amorphization is illustrated in parts C and D in Figure 7, respectively. The additional coherency strain and interfacial energy of the partially transformed state may be relieved by forming an amorphous surface phase or grain boundary phase between particles within an aggregate (Figure 7C). This can simultaneously lower the surface and strain energies, although it comes with an increase in volume free energy due to the formation of the amorphous phase. Further delithiation may result in complete amorphization. (Another configuration not shown in Figure 7 would have a amorphous film separating the crystals in order to relieve volume strain energy; this is analogous to the amorphous grain boundary and heterointerfacial films[27−29] and may have been observed by Chen et al.[43]) Finally, for small enough particles, complete transformation to the amorphous state may occur even at partial delithiation if the reduction of surface and strain energy is more than the increase in volume free energy (Figure 7D).

Each of these transformation pathways has specific implications for electrochemical performance in a practical battery system. One is that the often-cited limitation in crystalline olivines of "one-dimensional diffusion" (along the [010] lithium channel direction) may be moot, if lithium transport occurs primarily in an amorphous phase that is structurally isotropic. Another is that the relevant surface for any considerations of the influence of surface defects on electrochemical potential may be the amorphous rather than crystalline surface. Perhaps most importantly, the electrochemical response of olivines undergoing the complex phase transitions shown here is expected to be sample history dependent and inherently hysteretic. For example, the recent observation of single-phase particles in partially charged $LiFePO_4$ by Delmas,[44] which are in conflict with the observation of multiphase particles by Chen et al.,[43] may reflect differences in the extent of phase redistribution following delithiation (such as Figure 7, part A vs part B). And an example of hysteretic response is that the OCV values upon charge and upon discharge to the same lithium composition may not ever converge (Figure 3). Tuning nanoscale olivines to take advantage of disorder while minimizing possible detrimental effects may be a fruitful approach to improved materials.

To identify the actual transformation path(s) for nano-Li_xMPO_4, concurrent efforts in experimental and theoretical development are necessary. Among various modeling methods at different length and time scales, continuum-level models are promising to reveal general trends in phase transformation pathways of Li_xMPO_4 particles during delithiation/lithiation. For example, Johnson[45] considers spinodal decomposition confined in spherical particles in a generalized diffuse-interface (phase-field) model. Model calculations

(45) Johnson, W. C. *Acta Mater.* **2001**, *49*, 3463.
(46) Kobayashi, R.; Warren, J. A.; Carter, W. C. *Physica D* **2000**, *140*, 141.

show that the solubility limits of the phase-separating phases increase with decreasing particle size, which may account for the observed size dependence of miscibility gap in the $Li_{1-x}FePO_4/Li_yFePO_4$ nanometer-scale particles. We recently applied a phase-field model[46,47] that treats spatial variation of structural order ("crystallinity") in polycrystalline materials to predict the formation of intergranular amorphous films in ceramics and metallic alloys.[48,49] On the basis of this work, a modified model, which is specific to Li_xMPO_4 systems and incorporates the surface and stress effects on phase stability, is being developed to explain the experimental observations.[50]

Conclusions

A comparative study of the structural and phase changes taking place during electrochemical cycling of nanoscale (<100 nm) and conventional $Li_{1-x}MPO_4$ has been conducted. By measuring the SOC dependence and time dependence of the OCV and the coexisting phase content, it is shown that the phase transformation path differs significantly between the two types of materials. Coarse-grained $LiFePO_4$ (113 nm) is shown to undergo a conventional two-phase reaction in which crystalline $LiFePO_4$ and $FePO_4$ are the predominant coexisting phases. In nanoscale samples, we observe that coexisting crystalline phases have greater mutual solubility for lithium (reduced miscibility gap) and find that the appearance of each phase constrains the unit cell parameters of the other in a manner consistent with coherency stress effects. In addition, it is shown that the compositions of the crystalline phases are not constant within the miscibility gap as expected for simple two-phase coexistence and that at least one disordered phase is simultaneously present. Thus, the phase transformation path in nanoscale olivines during electrochemical cycling can be much more complex than previously thought. The possible paths, and their implications for electrochemical performance in rechargeable battery systems, are discussed.

Acknowledgment. This work was supported in part by United States Advanced Battery Consortium Project No. DE-FC26-05NT42403. N.M. acknowledges support by the Royal Thai Government Scholarship, and Y.-H.K. acknowledges support by Taiwan Merit Scholarship TMS-94-2-A-019.

CM801722F

(47) Warren, J. A.; Kobayashi, R.; Lobkovsky, A.; Carter, W. C. *Acta Mater.* **2003**, *51*, 6035.
(48) Tang, M.; Carter, W. C.; Cannon, R. M. *Phys. Rev. B* **2006**, *73*, 024102.
(49) Tang, M.; Carter, W. C.; Cannon, R. M. *Phys. Rev. Lett.* **2006**, *97*, 075502.
(50) Tang, M.; Huang, H.-Y.; Meethong, N.; Kao, Y.-H.; Carter, W. C.; Chiang, Y.-M. Materials Research Society Symposium Proceedings Spring 2008 Meeting, in press.